International Journal of Solids and Structures 51 (2014) 1390–1402

Contents lists available at ScienceDirect

International Journal of Solids and Structures

journal homepage: www.elsevier.com/locate/ijsolstr

Contact analysis in the presence of an ellipsoidal inhomogeneity within a half space

Koffi Espoir Koumi [a,b], Lv Zhao [a], Julien Leroux [b], Thibaut Chaise [a], Daniel Nelias [a,*]

[a] Université de Lyon, INSA-Lyon, LaMCoS UMR CNRS 5259, F69621 Villeurbanne, France
[b] SNECMA, Centre de Villaroche, 77550 Moissy Cramayel, France

ARTICLE INFO

Article history:
Received 30 September 2013
Received in revised form 25 November 2013
Available online 3 January 2014

Keywords:
Inhomogeneity
Inclusion
Anisotropy
Eigenstrain
Eshelby's equivalent inclusion method (EIM)
Contact Mechanics

ABSTRACT

Many materials contain inhomogeneities or inclusions that may greatly affect their mechanical properties. Such inhomogeneities are for example encountered in the case of composite materials or materials containing precipitates. This paper presents an analysis of contact pressure and subsurface stress field for contact problems in the presence of anisotropic elastic inhomogeneities of ellipsoidal shape. Accounting for any orientation and material properties of the inhomogeneities are the major novelties of this work. The semi-analytical method proposed to solve the contact problem is based on Eshelby's formalism and uses 2D and 3D Fast Fourier Transforms to speed up the computation. The time and memory necessary are greatly reduced in comparison with the classical finite element method. The model can be seen as an enrichment technique where the enrichment fields from the heterogeneous solution are superimposed to the homogeneous problem. The definition of complex geometries made by combination of inclusions can easily be achieved. A parametric analysis on the effect of elastic properties and geometrical features of the inhomogeneity (size, depth and orientation) is proposed. The model allows to obtain the contact pressure distribution – disturbed by the presence of inhomogeneities – as well as subsurface and matrix/inhomogeneity interface stresses. It is shown that the presence of an inclusion below the contact surface affects significantly the contact pressure and subsurfaces stress distributions when located at a depth lower than 0.7 times the contact radius. The anisotropy directions and material data are also key elements that strongly affect the elastic contact solution. In the case of normal contact between a spherical indenter and an elastic half space containing a single inhomogeneity whose center is located straight below the contact center, the normal stress at the inhomogeneity/matrix interface is mostly compressive. Finally when the axes of the ellipsoidal inclusion do not coincide with the contact problem axes, the pressure distribution is not symmetrical.

1. Introduction

From a fundamental point of view the presence of inhomogeneities in a matrix is very interesting for contact problems, first because it modifies the subsurface stress field, and also because it disturbes very significantly the contact pressure distribution. On one hand, for metallic materials, aluminum alloys or ceramics, failure mechanisms can be initiated by the presence of material impurities such as cavities, inclusions or precipitates. Inclusions can raise internal stresses, at the origin of fatigue cracks which in turn reduce the service life of mechanical components such as rolling elements (Voskamp, 1985; Nelias et al., 1999; Nugent et al., 2000; Vignal et al., 2003; Chen et al., 2008). On the other hand, in heterogeneous materials such as composite materials, the presence of inhomogeneities that are added to improve structural properties strongly affects the distribution of stresses including at the surface interface.

The disturbance field caused by the presence of an inhomogeneity embedded in an infinite space has been investigated by many authors (Eshelby, 1957, 1959, 1961; Willis, 1964; Walpole, 1967; Asaro and Barnett, 1975; Mura and Furuhashi, 1984). Eshelby (1957, 1959) was the first to initiate a method dealing with an inhomogeneity in an infinite space, which is called the 'Equivalent Inclusion Method' (EIM). Moschovidis and Mura (1975) extended this method to obtain the Eshelby's tensor for the exterior points of an ellipsoidal inclusion as a function of harmonic and bi-harmonic potentials. All these authors limited their analysis to an infinite body.

The analytical solutions for displacements, strains and stresses in a half-space are difficult to obtain. Many authors investigated the effect of inhomogeneities in a half-space subjected to a prescribed load. To solve the problem, some assumptions are usually made. Mindlin and Cheng (1950) considered a half-space containing a

* Corresponding author. Tel.: +33 4 72 43 84 90; fax: +33 4 72 43 89 13.
E-mail address: daniel.nelias@insa-lyon.fr (D. Nelias).

0020-7683/$ - see front matter © 2013 Elsevier Ltd. All rights reserved.
http://dx.doi.org/10.1016/j.ijsolstr.2013.12.035

Nomenclature

Letters

a^*	contact radius for contact problem
$a_1,\ a_2,\ a_3$	semi-axes of an ellipsoidal inhomogeneity
B^*_{ijkl}	influence coefficients that relating the stress σ_{ij} at point (x_1^3, x_2, x_3) to the constant eigenstrain at the point (x_1^k, x_2^k, x_3^k)
$C^M_{ijkl},\ C^I_{ijkl}$	elastic constants of the matrix and the inhomogeneity
e^0_{ij}	deviatoric part of ε^0_{ij}
$E^M,\ E^I$	Young's modulus of the matrix and the inhomogeneity
$E(\theta', k),\ F(\theta', k)$	elliptical integrals
h	distance between the two surfaces of the contacting bodies
I_{ijkl}	the fourth-order identity tensor
K^n	coefficients in the normal displacement at the contact surface due to the contact pressure
$k^M,\ k^I$	bulk modulus of the matrix and the inhomogeneity
$L_1,\ L_2,\ L_3$	lengths of the three sides of the matrix in EF model
M_{ij}	influence coefficients relating the stress σ_{ij} at the point (x_1, x_2, x_3) to the normal traction σ^n within a discretized area centered at $(x_1^k, x_2^k, 0)$
$n_1,\ n_2,\ n_3$	grid number in the half-space along the Cartesian directions $x_1,\ x_2,\ x_3$, respectively
P	normal applied load
P_0	maximum Hertzian pressure
p	contact pressure distribution
R	indenter radius
S_{ijkl}	components of the Eshelby's tensor
u^0_i	displacements corresponding to the strain applied at infinity ε^0_{ij}
u_i	disturbed contribution of the displacements
W	applied exterior load
dx_3	depth of the inclusion from the surface of the matrix in EF model
$x^I = (x_1^I, x_2^I, x_3^I)$	Cartesian coordinates of the inclusion center

Greek letters

ε^0_{ij}	infinite applied strain
ε_{ij}	strain due to eigenstrains
ε^*_{ij}	eigenstrain due to the presence of inhomogeneities
ε^0_{kk}	spherical part of ε^0_{ij}
ε^p	initial eigenstrain of the inhomogeneity
σ^0_{ij}	stress corresponding to the infinite applied strain ε^0_{ij}
σ_{ij}	disturbed contribution of the stresses
$\phi,\ \Psi$	harmonic and biharmonic potentials of mass density ε^*_{ij}
$\phi_{ij..}, \Psi_{ij..}$	harmonic and biharmonic potentials of mass density $x_i x_j \ldots$
δ_{ij}	Kronecker symbol
σ^n	normal pressure due to the summation of both symmetric inclusions
$\Delta x_1,\ \Delta x_2$	half size of the discretized surface area
$\nu^M,\ \nu^I$	Poisson's ratio of the matrix M and the inclusion I
$\mu^M,\ \mu^I$	shear modulus of the matrix and the inclusion
γ	the ratio of the inhomogeneity's Young's modulus to the matrix's
δ	the ratio of the inhomogeneity's bulk modulus to the matrix's
η	the ratio of the inhomogeneity's shear modulus to the matrix's
θ	the tilt angle of the inhomogeneity in the x_1Ox_3 plan

Acronyms and fast Fourier transforms

2D-FFT	two-dimensional fast Fourier transform
3D-FFT	three-dimensional fast Fourier transform
FFT^{-1}	inverse FFT operation
$\widehat{B}_{ijkl}$	frequency response of coefficients B_{ijkl} in the frequency domain
$\widehat{M}_{ij}$	frequency response of coefficients M_{ij} in the frequency domain

hydrostatic eigenstrain; Aderogba (1976) assumed a spherical inclusion with an arbitrary eigenstrain; Chiu (1977, 1978) limited his analysis to a cuboidal inclusion with an incompressible eigenstrain; Seo and Mura (1970) assumed an ellipsoidal inclusion with a pure dilatational eigenstrain.

Meanwhile, for the exterior points of the ellipsoidal inclusion in an infinite space, the Eshelby's tensor was expressed in terms of the harmonic and bi-harmonic potentials of the inclusion (Mura et al., 1987). The potentials can also be written in terms of elliptical integrals.

Several authors already investigated stress concentration due to the presence of inclusions or inhomogeneities. However until very recently they did not solve the contact problem, instead they assumed the hertzian contact pressure distribution as input (see for example Kabo and Ekberg, 2002; Kabo and Ekberg, 2005 or Courbon et al., 2005). For the 2D contact problem the effect of the presence of an elliptical heterogeneous inclusion on the contact loading was first solved numerically by Kuo (2007) and Kuo (2008) using the Boundary Element Method (BEM). The effect of inhomogeneities on the three-dimensional contact problem solution was first investigated by Nelias and co-workers (Leroux et al., 2010; Leroux and Nelias, 2011) and then by Zhou et al. (2011a) based on the semi-analytical method (SAM) initially proposed by Jacq et al. (2002) to numerically solve 3D elastic–plastic contact. For more details on the modeling of inclusions in contact problems the reader may refer to the review paper by Zhou et al. (2013).

SAMs have been continuously developed since ten years, and then successfully applied to several leading edge problems such as thermo-elastic–plastic contact modeling (Boucly et al., 2005), modeling of plasticity and accumulation of plastic strains (Boucly et al., 2005; Wang et al., 2005), running-in (Nelias et al., 2007) and wear modeling (Gallego and Nelias, 2007; Gallego et al., 2006, 2010a,b), simulation of single impact (Chaise et al., 2011), shot peening (Chaise et al., 2012) and low plasticity burnishing (Nelias et al., 2007; Chen et al., 2008; Chaise and Nelias, 2011), modeling of cuboidal inclusions (Liu and Wang, 2005; Zhou et al., 2009, 2011a,b, 2012), as well as to account for material or coating anisotropy (Bagault et al., 2012, 2013). With the same technique (Wang et al., 2009) solved a contact between two joined quarter spaces and a rigid sphere.

In this paper, the analysis will be limited to a single elastic ellipsoidal inhomogeneity which can be anisotropic and with any orientation. This is one of the key steps for the modeling of contact for composite materials since fibers are mostly anisotropic. It should be outlined that the intent here is not to simulate the macroscopic response of the contact assuming homogenized and anisotropic material properties, as very recently studied by Rodriguez-Tembleque et al. (2013). The effects of Young's modulus, bulk coefficient and shear modulus will be first investigated. It will be shown that the presence of an heterogeneous inclusion will not only affect the local stress field, but also very significantly the contact pressure distribution. Finally the presence of an anisotropic

and ellipsoidal inclusion located below the surface and with its axes not coincident with the contact ones will be presented.

2. Contact problem formulation

Generally, the formulation of the normal contact between two finite bodies B_1 and B_2 (Fig. 1) consists in a set of equations and inequalities that are recalled below:

- The load balance. The applied load W and the integration of the contact pressure $p(x_1,x_2)$ in the contact region Γ_c must be strictly equal.

$$W = \int_{\Gamma_c} p(x_1,x_2)d\Gamma, \tag{1}$$

- The surface separation. The gap between the two contacting surfaces is:

$$h(x_1,x_2) = h_i(x_1,x_2) + \delta + u_3^{(B_1+B_2)}(x_1,x_2), \tag{2}$$

where $h_i(x_1,x_2)$ is the initial geometry, δ the rigid body displacement, and $u_3^{(B_1+B_2)}(x_1,x_2)$ the sum of normal displacements of surfaces 1 and 2, that can be due to elastic deflection (under loading only), plastic deformation or the presence of inhomogeneities.

- The contact conditions. The distance $h(x_1,x_2)$ is always positive, because the contacting bodies can not interpenetrate each other. The conditions are defined by the inequalities:

$$\begin{aligned} &h(x_1,x_2) \geqslant 0,\\ &\text{contact} : h_i(x_1,x_2) = 0 \quad \text{and} \quad p(x_1,x_2) > 0,\\ &\text{separation} : h_i(x_1,x_2) > 0 \quad \text{and} \quad p(x_1,x_2) = 0. \end{aligned} \tag{3}$$

3. Theoretical background – Eshelby's equivalent inclusion method in Contact Mechanics

Given that the presence of inhomogeneities creates an incompatibility of deformation between the inhomogeneities and the matrix, the Eshelby's equivalent inclusion method is used.

3.1. Eshelby's solution for an infinite space

An infinite matrix D with the elastic stiffness tensor C^M_{ijkl} containing an ellipsoidal domain Ω with the elastic stiffness tensor C^I_{ijkl} is submitted at infinity to a uniform strain ε^0. The strain field is disturbed by the presence of the inhomogeneity. The disturbed contributions of the stresses and displacements are denoted σ_{ij} and u_i respectively. The total stress is $\sigma_{ij}+\sigma^0_{ij}$ and the total displacement $u_i + u^0_i$.

The stress components are in self-equilibrium if one neglects the body forces:

$$\sigma_{ij,j} = 0 \tag{4}$$

and $\sigma_{ij} = 0$ at infinity.

Under the hypothesis of linear isotropic elasticity, the stress components are calculated by the Hooke's law:

$$\begin{aligned} &\sigma^0_{ij} + \sigma_{ij} = C^I_{ijkl}(u^0_{k,l} + u_{k,l}) = C^I_{ijkl}(\varepsilon^0_{kl} + \varepsilon_{kl}) \quad \text{in } \Omega,\\ &\sigma^0_{ij} + \sigma_{ij} = C^M_{ijkl}(u^0_{k,l} + u_{k,l}) = C^M_{ijkl}(\varepsilon^0_{kl} + \varepsilon_{kl}) \quad \text{in } D-\Omega. \end{aligned} \tag{5}$$

The Eshelby's equivalent inclusion method (EIM) consists in representing the ellipsoidal inhomogeneity as an inclusion having the same elastic properties C^M_{ijkl} as the matrix but being subjected to an additional imaginary strain called eigenstrain ε^* giving:

$$C^I_{ijkl}(\varepsilon^0_{kl} + \varepsilon_{kl}) = C^M_{ijkl}(\varepsilon^0_{kl} + \varepsilon_{kl} - \varepsilon^*_{kl}) \quad \text{in } \Omega. \tag{6}$$

The necessary and sufficient condition for the equivalence of the stresses and strains in the two above problems of inhomogeneity and inclusion is provided by Eq. (6). In particular, the eigenstrain ε^*_{ij} is related to compatibility strain ε_{ij} by:

$$\varepsilon_{ij} = S_{ijkl} \times \varepsilon^*_{kl}, \tag{7}$$

where S_{ijkl} is the Eshelby's tensor.

Substitution of Eq. (7) into Eq. (6) leads to:

$$\Delta C_{ijkl} S_{klmn} \varepsilon^*_{mn} + C^M_{ijkl}\varepsilon^*_{kl} = -\Delta C_{ijkl}\varepsilon^0_{kl}, \tag{8}$$

where

$$\Delta C_{ijkl} = C^I_{ijkl} - C^M_{ijkl}.$$

When the inhomogeneity contains an initial eigenstrain ε^p (inhomogeneous inclusion), previous equations (Eq. (6)–(8)) are modified as follows.

$$\begin{aligned} &\sigma^0_{ij} + \sigma_{ij} = C^I_{ijkl}(\varepsilon^0_{kl} + \varepsilon_{kl} - \varepsilon^p_{kl}) \quad \text{in } \Omega,\\ &\sigma^0_{ij} + \sigma_{ij} = C^M_{ijkl}(\varepsilon^0_{kl} + \varepsilon_{kl}) \quad \text{in } D-\Omega. \end{aligned} \tag{9}$$

Using the EIM it yields,

$$C^I_{ijkl}(\varepsilon^0_{kl} + \varepsilon_{kl} - \varepsilon^p) = C^M_{ijkl}(\varepsilon^0_{kl} + \varepsilon_{kl} - \varepsilon^p_{kl} - \varepsilon^*_{kl}). \tag{10}$$

Hence,

$$\sigma_{ij} = C^I_{ijkl}(S_{klmn}\varepsilon^{**}_{mn} - \varepsilon^p) = C^M_{ijkl}(S_{klmn}\varepsilon^{**}_{mn} - \varepsilon^{**}_{kl}), \tag{11}$$

where

$$\varepsilon^{**} = \varepsilon^* + \varepsilon^p.$$

3.2. Determination of compatibility strain

The Eshelby's solution is only valid for a uniformly applied strain. However, the contact problem involves nonuniform strains.

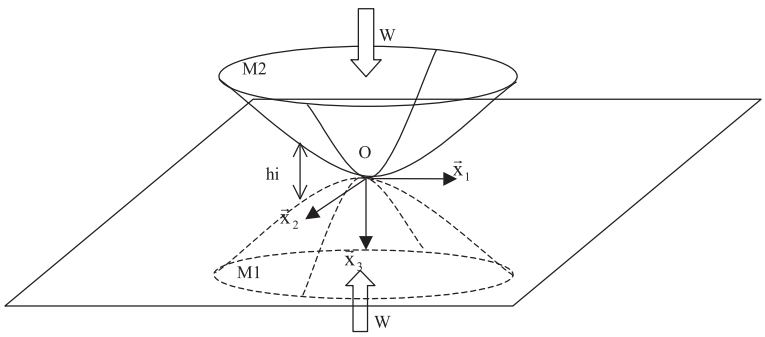

Fig. 1. Contact problem description.

Moschovidis and Mura (1975) have extended the Eshelby's EIM for nonuniformly applied strain. When the applied strain is a n-order polynomial, the equivalent eigenstrain is also treated as a n-order polynomial.

Considering an ellipsoidal inhomogeneity, if the applied strain is given by:

$$\varepsilon^0_{ij}(x) = E^0_{ij} + E^0_{ijk}x_k + E^0_{ijkl}x_k x_l + \cdots, \tag{12}$$

where the coefficients E^0 are constant, then the eigenstrain is assumed to be:

$$\varepsilon^*_{ij}(x) = B_{ij} + B_{ijk}x_k + B_{ijkl}x_k x_l + \cdots \tag{13}$$

The strain associated to the eigenstrain is given as:

$$\varepsilon_{ij}(x) = D_{ijkl}(x)B_{kl} + D_{ijklq}(x)B_{klq} + D_{ijklqr}(x)B_{klqr} + \cdots \tag{14}$$

For the interior points of an ellipsoidal inhomogeneity, the coefficients D_{ijkl} are constant and D_{ijklq} are linear in x. The expressions for D_{ijkl}, D_{ijklq}, D_{ijklqr} are given in Mura et al. (1987).

The results presented here are limited to a uniform eigenstrain, therefore, only the calculation of the tensor D_{ijkl} is performed.

$$D_{ijkl} = \frac{1}{8\pi(1-\nu)}[\Psi_{,ijkl} - 2\nu\delta_{kl}\phi_{,ij} - (1-\nu)(\delta_{kl}\phi_{il} + \delta_{ki}\phi_{jl} + \delta_{jl}\phi_{,ik} + \delta_{li}\phi_{jk})], \tag{15}$$

$$\Psi(x) = \int_\Omega |x - x'|dx',$$

$$\phi(x) = \int_\Omega \frac{1}{|x - x'|}dx'.$$

The harmonic potential $\phi(x)$ and the biharmonic potential $\Psi(x)$ can be expressed as a function of the elliptical integrals $E(\theta', k)$ and $F(\theta', k)$ (Gradshteyn, 1965), where:

$$E(\theta', k) = \int_0^{\theta'} (1 - k^2 sinw)^{1/2} dw,$$

$$F(\theta', k) = \int_0^{\theta'} \frac{1}{(1 - k^2 sinw)^{1/2}} dw, \tag{16}$$

$$\theta' = \sin^{-1}\left(1 - \frac{a_3^2}{a_1^2}\right)^{1/2},$$

$$k = \frac{3(a_1^2 - a_2^2)}{(a_1^2 - a_3^2)}. \tag{17}$$

Assuming that $a_1 > a_2 > a_3$, with a_1, a_2, a_3 the semi-axes of the ellipsoidal inclusion. The Eshelby's tensor S_{ijkl} is obtained from Eq. (15) as:

$$S_{ijkl} = D_{ijkl}(x^I), \tag{18}$$

where $x^I = (x^I_1, x^I_2, x^I_3)$ represents the cartesian coordinates of the inclusion center.

3.3. Half-space solution

Three dimensional contact problems involve a half-space that is bounded by the surface plane $x_3 = 0$ in the cartesian coordinate system (x_1, x_2, x_3). Mura et al. (1987) introduced a method to determine the eigenstrain. The obtained equations, despite of their complexity, are valid only in the case of hydrostatic eigenstrains. In order to get rid of this restrictive hypothesis which is incompatible with the contact problem, Zhou et al. (2009) proposed an ingenious method allowing to extend the previous solution, valid only for infinite spaces, to half spaces. The solution for an isotropic half space consists in decomposing the problem into three subproblems (Fig. 2), known as Chiu's decomposition (Chiu, 1978).

(1) An inclusion with the prescribed eigenstrain $\varepsilon^* = (\varepsilon^*_{11}; \varepsilon^*_{22}; \varepsilon^*_{33}; \varepsilon^*_{12}; \varepsilon^*_{13}; \varepsilon^*_{23})$ in an infinite space.
(2) A symmetric inclusion with a mirror eigenstrain $\varepsilon^*_s = (\varepsilon^*_{11}; \varepsilon^*_{22}; \varepsilon^*_{33}; \varepsilon^*_{12}; -\varepsilon^*_{13}; -\varepsilon^*_{23})$ in the same space.
(3) A normal traction distribution $-\sigma^n$ at the surface of the half space ($x_3 = 0$) which is a function of the eigenstrains ε^* and ε^*_s.

The summation of the two solutions (1) and (2) leaves the plane of symmetry ($x_3 = 0$) free of shear tractions. By adding an opposite normal stress σ^n, the condition of free surface traction is obtained. The stress at any point of the domain meshed with $n_1 \times n_2 \times n_3$ cuboids is given by:

$$\begin{aligned}\sigma_{ij}(x_1,x_2,x_3) = &\sum_{x^I_3=0}^{n_3-1}\sum_{x^I_2=0}^{n_2-1}\sum_{x^I_1=0}^{n_1-1} B_{ijkl}(x_1 - x^I_1, x_2 - x^I_2, x_3 - x^I_3)\varepsilon^*_{kl}(x^I_1, x^I_2, x^I_3) \\ &+ \sum_{x^I_3=0}^{n_3-1}\sum_{x^I_2=0}^{n_2-1}\sum_{x^I_1=0}^{n_1-1} B_{ijkl}(x_1 - x^I_1, x_2 - x^I_2, x_3 + x^I_3)\varepsilon^*_{skl}(x^I_1, x^I_2, -x^I_3) \\ &- \sum_{x^I_2=0}^{n_2-1}\sum_{x^I_1=0}^{n_1-1} M_{ij}(x_1 - x^I_1, x_2 - x^I_2, x_3)\sigma^n(x^I_1, x^I_2, 0),\end{aligned} \tag{19}$$

where B_{ijkl} are the influence coefficients that relate the constant eigenstrain at the point (x^I_1, x^I_2, x^I_3) which is the inclusion center in an infinite space to the stress σ_{ij} at the point (x_1, x_2, x_3). M_{ij} represent the influence coefficients relating the normal traction σ^n within a discretized area centered at $(x^I_1, x^I_2, 0)$ to the stress σ_{ij} at the point (x_1, x_2, x_3).

$$B_{ijkl}(x) = C^M_{ijmn}D_{mnkl}(x) \quad \text{for } x \text{ in } D - \Omega, \tag{20}$$

$$B_{ijkl}(x) = C^M_{ijmn}(D_{mnkl}(x) - I_{mnkl}) \quad \text{for } x \text{ in } \Omega, \tag{21}$$

where $I_{ijkl} = \frac{1}{2}(\delta_{il}\delta jk + \delta_{ik}\delta jl)$is the fourth-order identity tensor.

For a single inclusion centered at (x^I_1, x^I_2, x^I_3) in the half-space, the normal traction σ^n at the surface point $(x'_1, x'_2, 0)$ is obtained as:

$$\begin{aligned}\sigma^n(x'_1, x'_2, 0) = &-B_{33kl}(x'_1 - x^I_1, x'_2 - x^I_2, -x^I_3,)\varepsilon^*_{kl}(x^I_1, x^I_2, x^I_3) \\ &- B_{33kl}(x'_1 - x^I_1, x'_2 - x^I_2, x^I_3,)\varepsilon^*_{skl}(x^I_1, x^I_2, -x^I_3).\end{aligned} \tag{22}$$

In Eq. (19), each component $M_{ij}()$ is obtained by a double integration of the function $F_{ij}()$ over a discretized surface area $2\Delta x_1 \times 2\Delta x_2$ centered at $(x^I_1, x^I_2, 0)$, see Appendices A and B .

$$M_{ij}(x_1 - x^I_1, x_2 - x^I_2, x_3) = \int_{x^I_1 - \Delta x_1}^{x^I_1 + \Delta x_1}\int_{x^I_2 - \Delta x_2}^{x^I_2 + \Delta x_2} F_{ij}(x_1 - x'_1, x_2 - x'_2, x_3)dx'_1x'_2. \tag{23}$$

The 3D-FFT is used to accelerate the calculation of the first (1) and second terms (2) and the 2D-FFT for the third term (3). Wrap around order and zero-padding techniques are used in order to remove the induced periodicity error (Liu et al., 2000).

3.4. Normal displacement of a surface point

The surface normal 'eigen-displacements' can be obtained when inserting the eigenstrain into the total strain. They are generated by the pressure field σ^n only. The normal displacements are calculated as:

$$u_3(x_1, x_2) = \sum_{x'_2=0}^{n_2-1}\sum_{x'_1=0}^{n_1-1} K^n(x_1 - x'_1, x_2 - x'_2)\sigma^n(x'_1, x'_2). \tag{24}$$

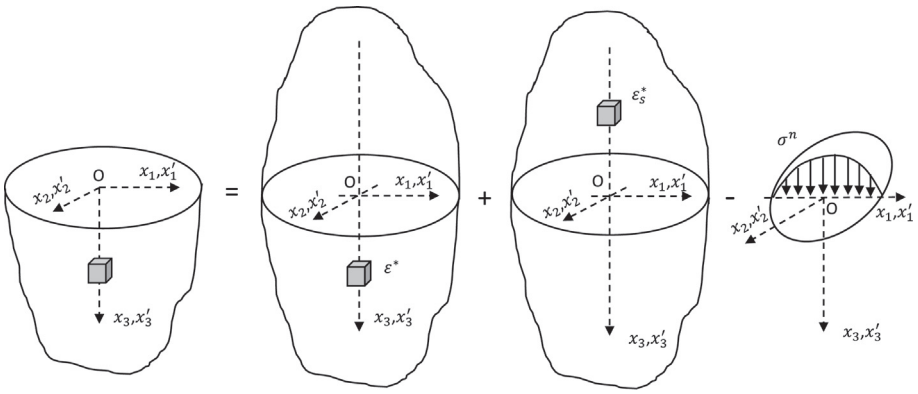

Fig. 2. Decomposition of the half-space solution into three sub-problems.

To solve the equation above numerically, the surface in contact is discretized into $n_1 \times n_2$ rectangular elements of uniform size $2\Delta x_1 \times 2\Delta x_2$. Then, pressure and displacement within each discrete patch are treated as constant and their values located at the center. The effect of an uniform pressure on a rectangular area has been given by Love et al. (1952) and Johnson (1985). K^n denotes the influence coefficients that relate the normal pressure at the surface point $(x_1', x_2', 0)$ to the normal displacement at the surface point $(x_1, x_2, 0)$, recalled in Appendix C.

4. Integration of the inhomogeneity effects in the contact algorithm

In order to integrate the inhomogeneity effects in the contact algorithm, an equivalent elastic algorithm is proposed, as shown in Fig. 3. The left frame in red presents the calculation of displacements due to the eigenstrain and the right frame in blue the ones due to the contact pressure. The effect of an inclusion on the contact problem derives from the fact that the surface contact geometry is modified by the eigen-displacement produces by the eigenstrain. The contact pressure and shears are then updated, which modifies the eigenstrain value. The elastic displacements are obtained from the updated contact pressure via the resolution of the elastic contact problem. The algorithm is repeated until convergence of the normal displacements is obtained.

It should be noted that in the frictional contact between dissimilar elastic materials, the tangential displacements of the surface points, as analyzed by Fulleringer et al. (2010) in analytical form for a cuboid of uniform eigenstrain, should be considered.

5. How to consider the orientation of an ellipsoidal inclusion

In order to take into account the orientation of the inclusion (Fig. 4), it is necessary to respect the three rules described below.

- Chiu's decomposition: Given that the orientations of the source inclusion and the mirror inclusion are different, the influence coefficients of the two inclusions are consequently different. However, the Chiu's symmetry permits to offset the effect of the shear stresses on the free surface.
- The Wrap Around: In the Wrap Around technique, the extension of the zone should be considered. Based on the symmetries, this technique is only valid in the inclusion's coordinate system, which implies a development of new coefficients of

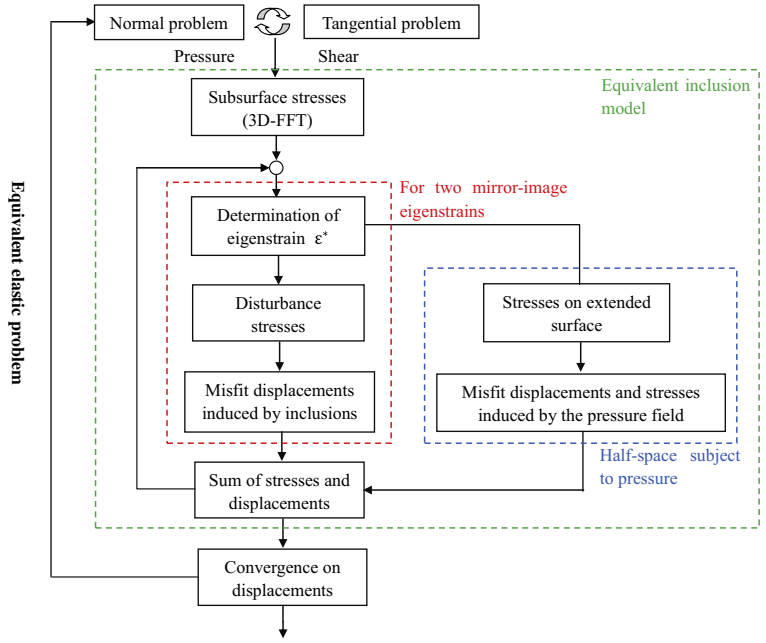

Fig. 3. Flowchart of the algorithm for the equivalent elastic problem.

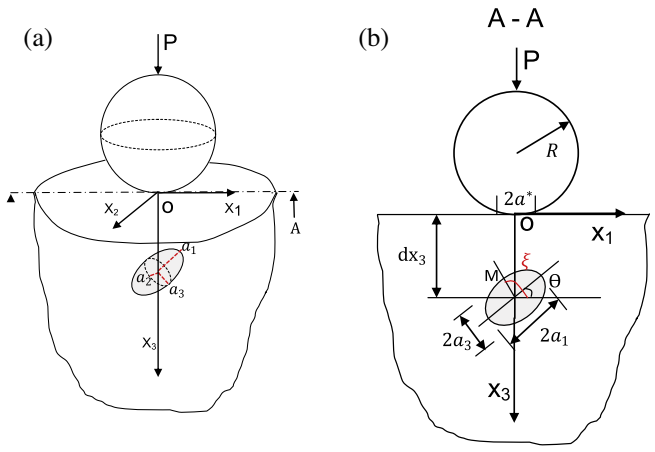

Fig. 4. Contact of a sphere over a flat in the presence of an arbitrarily oriented inclusion. (a) 3D configuration and (b) 2D configuration.

symmetries. On each mesh point of the contact coordinate system, it is necessary to associate a corresponding image point in the inclusion coordinate system and the corresponding coefficient of symmetry.

- The third step consists in taking into account the correct change of coordinate both for the source inclusion and the mirror inclusion. Hence, two transition matrixes based on the *ZXZ* convention of Euler angles are introduced, one for the source inclusion and the other one for the mirror inclusion.

It should be noted that this model is valid whatever the contacting surface geometry is, in other words it is not limited to the contact of a sphere and a flat.

6. Validation by finite element analysis

In order to validate the semi-analytical method, a comparison with a finite element (FE) model was performed using the commercial FE package Abaqus v6.11.

The configuration is shown in Fig. 5. A contact between a sphere and a plane (solid) containing an ellipsoidal inclusion at a certain depth (dx_3) is described. In order to correctly describe the interface, the inclusion is obtained by making a solid partition in a local coordinate system related to the contact coordinate, via a rotation of 30 degrees around the x_2 axis (Fig. 6). The size of the sphere and the solid are recalled in Table 1. The geometrical properties and position of the inclusion are normalized by the contact half-width a^*, as shown in Table 2.

Since the model is symmetric with respect to the plane $x_2 = 0$, only half of the bodies in contact are meshed. The solid is clamped on the lower surface, the sphere can just move vertically. A point force is applied on the sphere generating a half-width of contact of 1 mm (from Hertzian theory). The latter is much smaller compared with the radius of the sphere (1/31) such that the half-space assumption (i.e. the contact size should be small compared to the dimensions of the bodies in contact) is satisfied. A local area called 'subsurface layer' is meshed by 30,250 linear hexahedral elements (C3D8) of size $0.02a^*$, while the rest of solid is meshed with 1,088,349 linear tetrahedral (C3D4) elements. The (quarter) sphere contains 39,671 quadratic tetrahedral (C3D10) elements and the inclusion 11,009 linear tetrahedral (C3D4) elements.

Three calculations are carried out. The first case corresponds to an homogeneous body to be compared with the Hertz's solution. The second case considers an isotropic tilted inclusion and is used to validate the framework for the inclusion orientation. At last, the third case considers an orthotropic elastic inclusion, for which the orthotropic coordinate system coincides with the contact coordinate system.

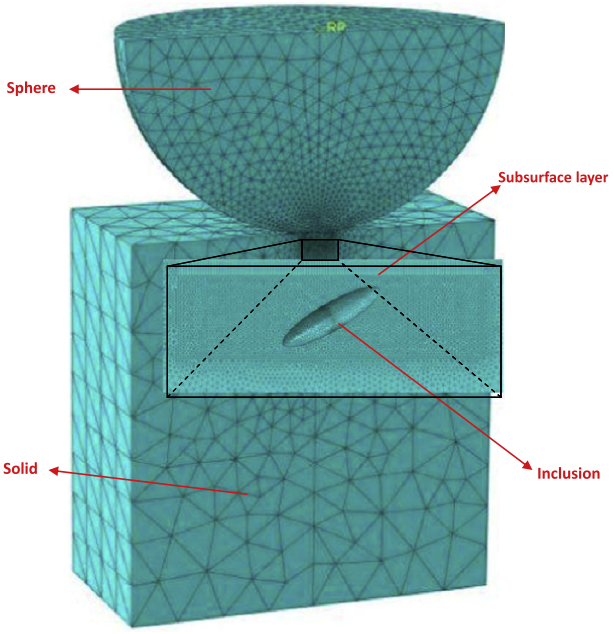

Fig. 5. Finite element model used for the validation.

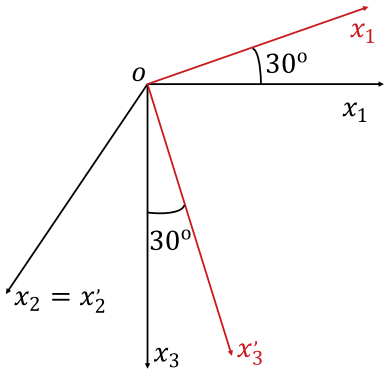

Fig. 6. Local coordinate system for the model partition.

Table 1
Geometry of the bodies in contact.

Region	Geometry (mm)
Sphere	$R = 31$
Solid	$L_1 = L_2 = L_3 = 60$

Table 2
Size and location of the ellipsoidal inclusion (reference case).

Geometry	Position
$a_1 = 0.4a^*,\ a_2 = a_3 = 0.1a^*$	$dx_3 = 0.4a^*$

The material properties for each region of the model and for each case are shown in Table 3.

Results from the Semi Analytical Method and the Finite Element Model are presented in Fig. 7 for the three cases studied. The comparison focuses on pressure distribution obtained by both methods. An excellent agreement is observed between both methods thus validating the SAM framework.

7. Parametric study

In this section, a normal contact between a spherical indenter and an elastic half space containing a single inhomogeneity is considered. The radius of the indenter is $R = 62$ mm and the normal force $P = 10,000$ N. The Young's modulus and Poisson's ratio for the half space are chosen as $E^M = 210$ GPa and $\nu^M = 0.3$ respectively (the equivalent bulk modulus and shear modulus are $k^M = 175$ GPa and $\mu^M = 80.77$ GPa). The resulting contact width and maximum contact pressure for the homogeneous half-space, given by Hertz theory, are: $2a^* = 2$ mm and $P_0 = 4750$ MPa. An ellipsoidal inhomogeneity with semi-axes $a_1 = 0.4a^*$, $a_2 = 0.1a^*$, $a_3 = 0.1a^*$ and its center located at $dx_3 = 0.3a^*$ will be considered.

7.1. Isotropic inhomogeneity

The effect of an isotropic inhomogeneity on the contact pressure distribution and the subsurface stress field is here investigated. The analysis will be subdivided into three cases:

- Effect of the Young's moduli ratio $\gamma = E^I/E^M$ for $\nu^I = \nu^M = 0.3$.
- Effect of the bulk moduli ratio $\delta = k^I/k^M$ for $\mu^I = \mu^M = 80.77$ GPa.
- Effect of the shear moduli ratio $\eta = \mu^I/\mu^M$ for $k^I = k^M = 175$ GPa.

7.1.1. Effect of the Young's modulus

The Poisson's ratio of the inhomogeneity is chosen as $\nu^I = 0.3$. For this case, the elastic moduli of the inhomogeneity are given as follows:

$$C^I_{ijkl} = \frac{E^I\nu^I}{(1+\nu^I)(1-2\nu^I)}\delta_{ij}\delta_{kl} + \frac{E^I}{(1+\nu^I)}(\delta_{ik}\delta_{jl} + \delta_{il}\delta_{jk}), \tag{25}$$

$$\nu^I = \nu_M \quad \text{and} \quad E^I = \gamma E^M, \tag{26}$$

$$C^I_{ijkl} = \gamma C^M_{ijkl},$$

$$\Delta C = C^I_{ijkl} - C^M_{ijkl} = (\gamma - 1)C^M_{ijkl}. \tag{27}$$

Eq. (10) becomes:

$$(\gamma - 1)C^M_{ijkl}S_{klmn}\varepsilon^*_{mn} + C_{ijkl}\varepsilon^*_{kl} = (1-\gamma)C^M_{ijkl}\varepsilon^0_{kl}. \tag{28}$$

The dimensionless contact pressure distribution is presented for different values of γ in Fig. 8. The case of an inclusion parallel to the surface is presented in Fig. 8(a) ($\theta = 0$). Fig. 8(b) presents the case for $\theta = 45^\circ$.

It can be observed that the magnitude of the contact pressure increases when the inclusion becomes stiffer, i.e. when $\gamma > 1$. Conversely when the inclusion is softer than the matrix, i.e. $\gamma < 1$, the substrate material surrounding the inhomogeneity becomes more compliant and the contact pressure gets smaller than the Hertzian pressure. Meanwhile the contact area increases. In Fig. 8(a), $\gamma \to \infty$ corresponds to a peak magnitude augmentation of 24.3% while $\gamma \to 0$ leads to a reduction of 32.12%, compared with the homogeneous half space $\gamma = 1$. For an inclined rigid inclusion ($\gamma \to \infty$ and $\theta = 45^\circ$, see Fig. 8(b)) it should be noticed a sharp increase of the maximum contact pressure which is here five times the Hertz's solution. Note also that when the inclusion becomes infinitely soft ($\gamma \to 0$), as for a void or cavity, the pressure drops locally to zero.

The influence of the orientation angle is observed for the case of a stiff inclusion ($\gamma = 4$) in Fig. 9. When $\theta \neq 0$ both the surface pressure and stress component lose their symmetry in the plane $x_1 = 0$. When θ approaches 90°, the inhomogeneity gets very closed to the surface and the peak magnitude of the contact pressure increases by more than 245.47%, compared with the case $\theta = 0$.

In Fig. 10(a) and (b), the effect of the inhomogeneity's center location on the contact pressure distribution is shown. When its dimensionless depth (dx_3/a^*) is greater than 0.7, the effect of the inhomogeneity on the contact pressure distribution becomes negligible.

The effect of the inhomogeneity on the subsurface stresses is now investigated and the results are presented in Figs. 11 and 12. As a general trend it is observed that the stress components (σ_{ij}) inside the inhomogeneity increase as the inhomogeneity becomes stiffer and at the contrary decrease as the inhomogeneity becomes more compliant.

The stress at the interface between the inclusion and the matrix is of great interest to study crack initiation or debonding of composite's fibers. When the point M describes the inclusion matrix interface (see Fig. 4(b)), the angle ξ ranges from 0° to 360°. Figs. 13 and 14 show the normal and shear stresses at the inhomogeneity/matrix interface as a function of the angle ξ (the position of the point M at this interface) for three different Young's moduli ratios γ. Note that the normal stress is almost always negative which means compressive. One can remark that the normal shear stress at the inhomogeneity/matrix interface increases when the inhomogeneity becomes stiffer. For the asymptotic case of a rigid inclusion (i.e. when $\gamma \to \infty$) the maximum value of the interfacial shear stress reached $0.69P_0$ in the case of the ellipsoidal inhomogeneity (Fig. 13) while it becomes slightly higher ($0.86P_0$) in the case of a spherical inhomogeneity (Fig. 14).

7.1.2. Effect of the bulk modulus

The effect of the bulk modulus on the contact problem is now investigated. The bulk modulus characterizes the volume variation. The inhomogeneity and matrix shear moduli are set equal ($\mu^I = \mu^M = 80.77$ GPa). Note that in the case of a spherical inhomogeneity, the eigenstrain is purely hydrostatic. $\delta = k^I/k^M$ is the ratio of the inhomogeneity's bulk modulus to the matrix one. In particular, $\delta \to \infty$ and $\delta \to 0$ correspond to a Poisson's ratio of 0.5 (i.e. incompressible) and -1 for the inhomogeneity, respectively.

Since C_{ijkl} is an isotropic tensor, C^I can be decomposed in the base of isotropic tensors J and K.

$$C^I_{ijkl} = 3k^I J_{ijkl} + 2\mu^I K_{ijkl}, \tag{29}$$

Table 3
Material properties for each region and for each case

Region		Material properties		
Sphere		$E^S = 10^{10}$ GPa,		$\nu^S = 0.3$
Solid		$E^M = 210$ GPa,		$\nu^M = 0.3$
Inhomogeneity	Case 1 (Isotropic)	$E^I = 210$ GPa,		$\nu^I = 0.3$
	Case 2 (Isotropic)	$E^I = 840$ GPa,		$\nu^I = 0.3$
	Case 3 (Orthotropic)	$E^I_1 = 210$ GPa,	$E^I_2 = 623$ GPa,	$E^I_3 = 50$ GPa
		$\mu^I_{12} = 83$ GPa,	$\mu^I_{13} = 400$ GPa,	$\mu^I_{23} = 20$ GPa
		$\nu^I_{12} = 0.15$,	$\nu^I_{13} = 0.26$,	$\nu^I_{23} = 0.40$

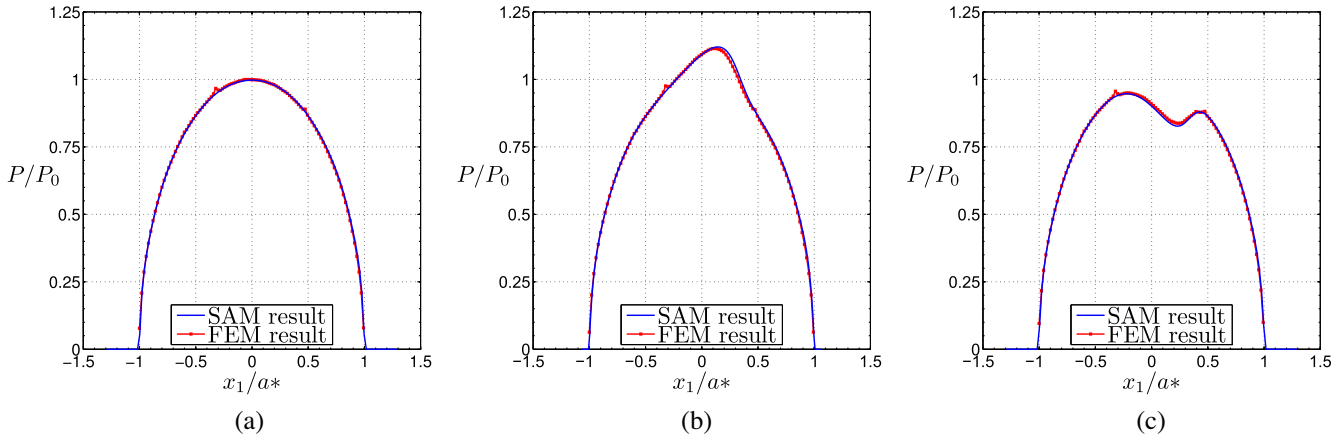

Fig. 7. Comparison between the Semi Analytical Method (SAM) and the FEM; (a) Hertzian contact, (b) isotropic tilted inhomogeneity, and (c) orthotropic tilted inhomogeneity.

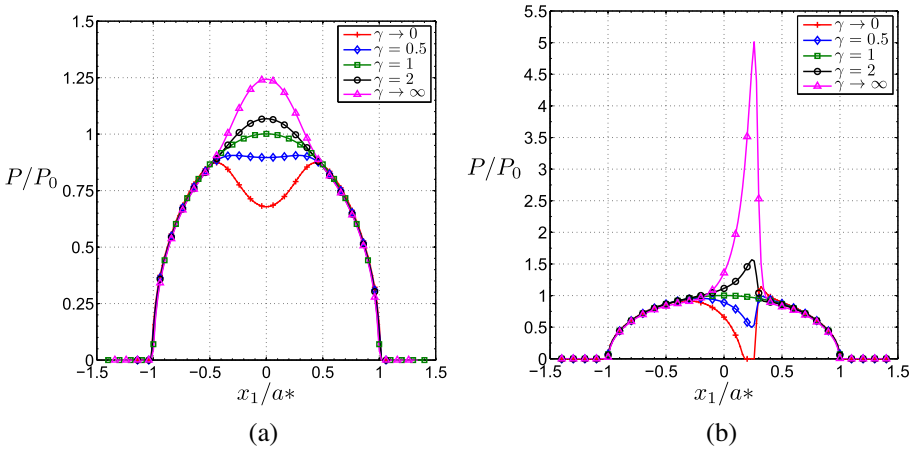

Fig. 8. Effect of the dimensionless Young's modulus $\gamma = E^I/E^M$ (with $\nu^I = \nu^M = 0.3$) on the dimensionless contact pressure distribution for isotropic ellipsoidal inclusion ($a_1 = 0.4a^*,\ a_2 = a_3 = 0.1a^*,\ dx_3 = 0.3a^*$); (a) $\theta = 0$ and (b) $\theta = 45^\circ$.

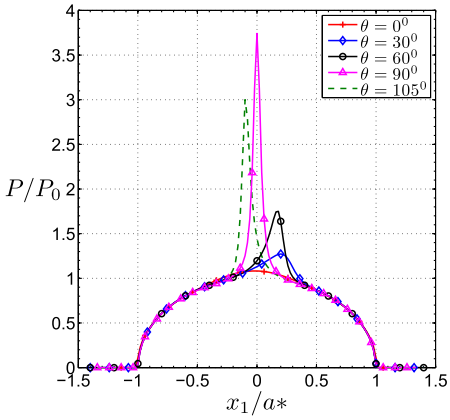

Fig. 9. Dimensionless contact pressure distribution for different orientation angles θ for a stiff ($\gamma = 4$) isotropic ellipsoidal inclusion ($a_1 = 0.4a^*,\ a_2 = a_3 = 0.1a^*,\ dx_3 = 0.4a^*$).

where

$J_{ijkl} = \frac{1}{3}\delta_{ij}\delta_{kl}$ and $K_{ijkl} = I_{ijkl} - J_{ijkl}$

$I_{ijkl} = \frac{1}{2}(\delta_{il}\delta_{jk} + \delta_{ik}\delta_{jl})$, is the fourth-order identity tensor

$J_{ijkl}\varepsilon_{kl} = \frac{\varepsilon_{kk}}{3}\delta_{ij}$(spherical part), and $K_{ijkl}\varepsilon_{kl} = e_{ij}$(deviatoric part)

$$\mu^I = \mu^M, \quad k^I = \delta k^M, \tag{30}$$

$$\Delta C = C^I - C^M = 3(k^I - k^M)J_{ijkl} = 3(\delta - 1)k^M J_{ijkl}. \tag{31}$$

Then Eq. (10) becomes

$$3(\delta - 1)k^M J_{ijkl}S_{klmn}\varepsilon^*_{mn} + C^M_{ijkl}\varepsilon^*_{kl} = -3(\delta - 1)k^M J_{ijkl}\varepsilon^0_{kl}, \tag{32}$$

$$(\delta - 1)k^M \delta_{ij}S_{kkmn}\varepsilon^*_{mn} + C^M_{ijkl}\varepsilon^*_{kl} = -(\delta - 1)k^M \delta_{ij}\varepsilon^0_{kk}, \tag{33}$$

where ε^0_{kk} represents the spherical part of ε^0_{kl}.

Fig. 15(a) and (b) present the dimensionless contact pressure distribution for various bulk moduli ratios δ. It can be observed that the contact pressure locally increases on the top of the inclusion when it tends to be incompressible (i.e. when k^I or $\delta \to \infty$). This peak of pressure is less marked when the ellipsoidal inclusion, which center is located at the dimensionless depth $dx_3/a^* = 0.3$, is oriented parallel to the surface ($\theta = 0$, Fig. 15(a)) whereas it becomes sharp for the inclined inclusion (Fig. 15(b)). This can be explained by the fact that in the latter configuration ($\theta = 45^\circ$) the surface of the inclusion becomes closer to the contact interface. Note that there is no need to have a stiff inclusion to increase the maximum contact pressure, a relatively soft but incompressible one will have a very similar behavior.

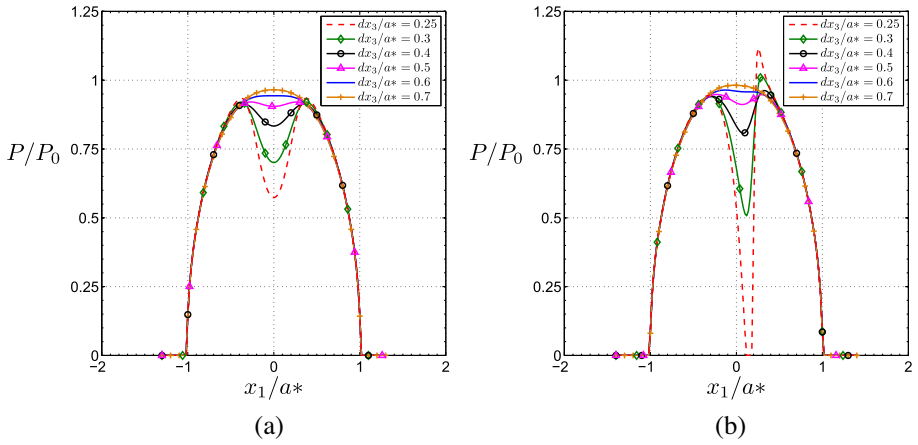

Fig. 10. Dimensionless contact pressure distribution for different dimensionless depths dx_3/a^* for an ellipsoidal cavity ($a_1 = 0.3a^*,\ a_2 = a_3 = 0.1a^*,\ \gamma \to 0$); (a) $\theta = 0$ and (b) $\theta = 45^\circ$.

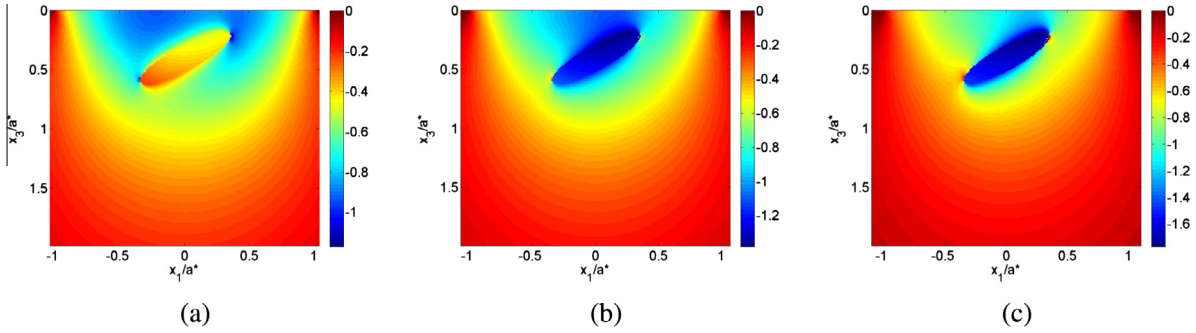

Fig. 11. σ_{33}/P_0 in the plane $x_2 = 0$ for various dimensionless Young's moduli $\gamma = E^I/E^M$ (with $\nu^I = \nu^M = 0.3$) for isotropic ellipsoidal inclusion ($a_1 = 0.4a^*,\ a_2 = a_3 = 0.1a^*,\ dx_3/a^* = 0.4,\ \theta = 30^\circ$); (a) $\gamma = 0.25$, (b) $\gamma = 4$, and (c) $\gamma \to \infty$.

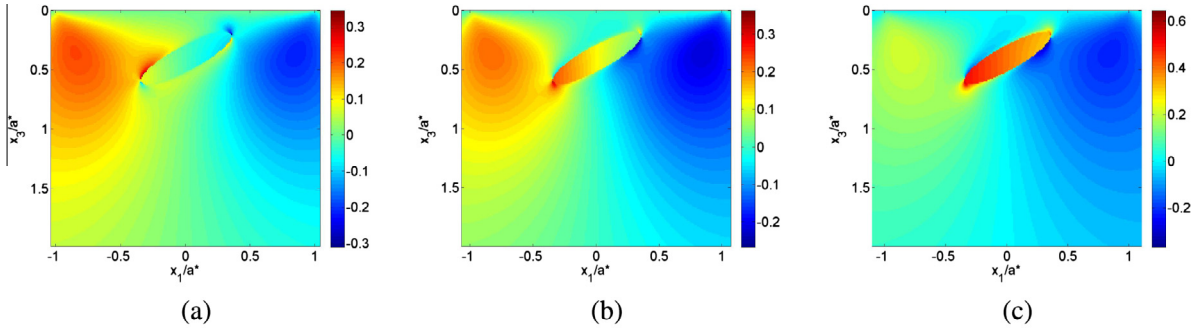

Fig. 12. σ_{13}/P_0 in the plane $x_2 = 0$ for various dimensionless Young's moduli $\gamma = E^I/E^M$ (with $\nu^I = \nu^M = 0.3$) for isotropic ellipsoidal inclusion ($a_1 = 0.4a^*,\ a_2 = a_3 = 0.1a^*,\ dx_3/a^* = 0.4,\ \theta = 30^\circ$); (a) $\gamma = 0.25$, (b) $\gamma = 4$, and (c) $\gamma \to \infty$.

7.1.3. Effect of the shear modulus

The bulk modulus of the inhomogeneity is chosen equal to the matrix one, $k^I = k^M = 175$ GPa. When the inhomogeneity is spherical, the eigenstrain is purely deviatoric. The ratio of the inhomogeneity's shear modulus to the matrix one is defined by the dimensionless parameter $\eta = \mu^I/\mu^M$.

The elastic modulus of the inhomogeneity is given as follow:

$$C^I_{ijkl} = 3k^I J_{ijkl} + 2\mu^I K_{ijkl}, \tag{34}$$

$$k^I = k^M, \quad \mu^I = \eta\mu^M, \tag{35}$$

$$\Delta C = C^I - C^M = 2(\eta - 1)\mu^M K_{ijkl}. \tag{36}$$

Eq. (10) becomes

$$2(\eta - 1)\mu^M K_{ijkl} S_{klmn}\varepsilon^* mn + C^M_{ijkl}\varepsilon^*_{kl} = -2(\eta - 1)\mu^M e^0_{ij}, \tag{37}$$

where e^0_{ij} represents the deviatoric part of ε^0_{ij}.

The effect of the dimensionless shear modulus, η, on the contact pressure distribution is shown in Fig. 16(a) and (b). It can be observed that variations of contact pressure for different values of γ (see Fig. 8) and η (see Fig. 16) are quite similar.

7.2. Anisotropic inhomogeneity

The material properties of the inhomogeneity are here taken anisotropic. An orthotropic material is considered. The elastic

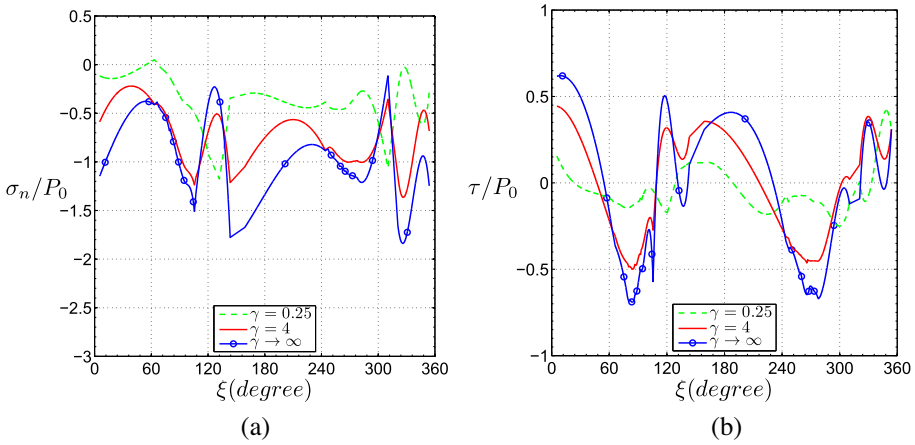

Fig. 13. Dimensionless normal and shear stresses (σ_n/P_0 and τ/P_0) in the plane $x_2 = 0$ for various dimensionless Young's moduli $\gamma = E^I/E^M$ in presence of a single isotropic ellipsoidal inclusion ($a_1 = 0.4a^*,\ a_2 = a_3 = 0.1a^*,\ dx_3/a^* = 0.4,\ \theta = 30^\circ$); (a) σ_n/P_0 and (b) τ/P_0.

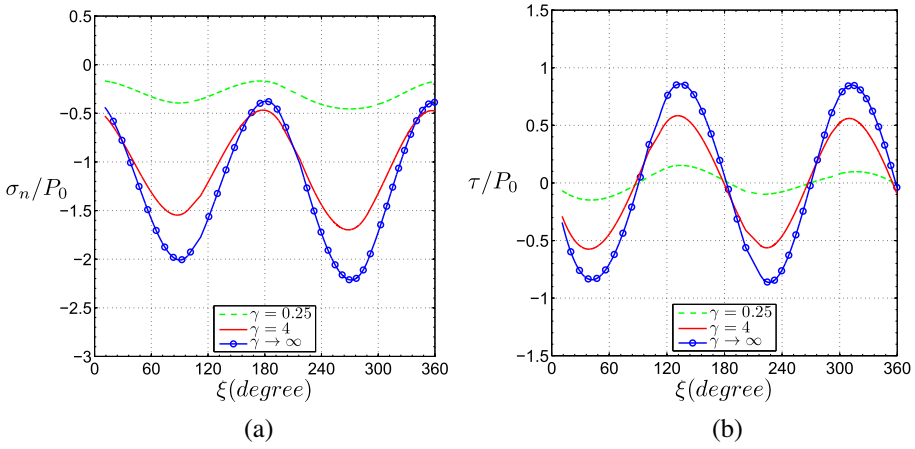

Fig. 14. Dimensionless normal and shear stresses (σ_n/P_0 and τ/P_0) in the plane $x_2 = 0$ for various dimensionless Young's moduli $\gamma = E^I/E^M$ in presence of a single isotropic and spherical inclusion ($a_1 = a_2 = a_3 = 0.2a^*,\ dx_3/a^* = 0.3$); (a) σ_n/P_0 and (b) τ/P_0.

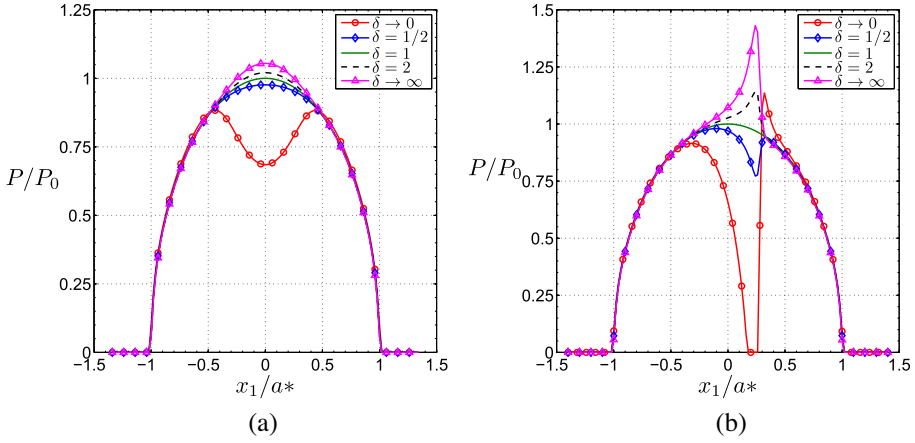

Fig. 15. Effect of the dimensionless bulk modulus $\delta = k^I/k^M$ on the dimensionless contact pressure distribution for a single isotropic ellipsoidal inclusion ($a_1 = 0.4a^*,\ a_2 = a_3 = 0.1a^*,\ dx_3 = 0.3a^*$); (a) $\theta = 0$ and (b) $\theta = 45^\circ$.

coefficients are given in the orthotropy axes $R_{orthotropic}$ as follows: $E_1^I = 210\,\text{GPa}$, $E_2^I = 623\,\text{GPa}$, $E_3^I = 50\,\text{GPa}$, $\mu_{12}^I = 83\,\text{GPa}$, $\mu_{13}^I = 400\,\text{GPa}$ $\mu_{23}^I = 20\,\text{GPa}$, $\nu_{12}^I = 0.15$, $\nu_{13}^I = 0.26$, and $\nu_{23}^I = 0.4$. The inclusion orientation θ is set equal to 45°.

Euler Angles of type ZXZ are introduced (Fig. 17) in order to define the orientation of the orthotropy using a combination of three rotations (φ, θ, ψ) around the axes of the contact reference frame (x_1, x_2, x_3).

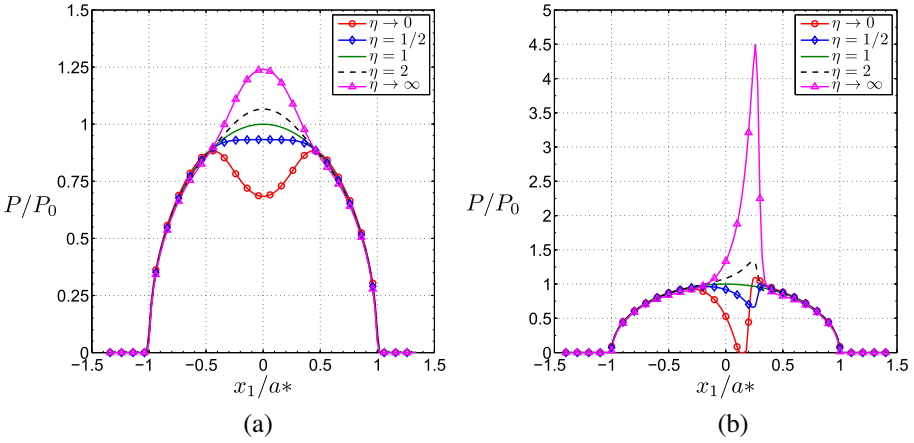

Fig. 16. Effect of the dimensionless shear modulus $\eta = \mu^I/\mu^M$ on the dimensionless contact pressure distribution for a single isotropic ellipsoidal inclusion ($a_1 = 0.4a^*,\ a_2 = a_3 = 0.1a^*,\ dx_3 = 0.3a^*$); (a) $\theta = 0$ and (b) θ=45°.

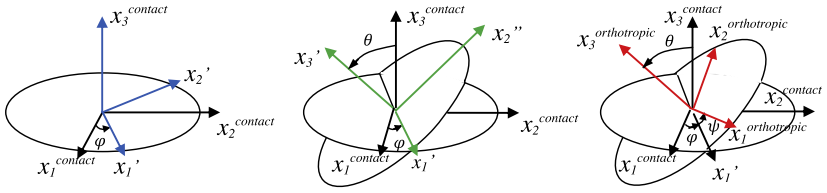

Fig. 17. Euler Angles.

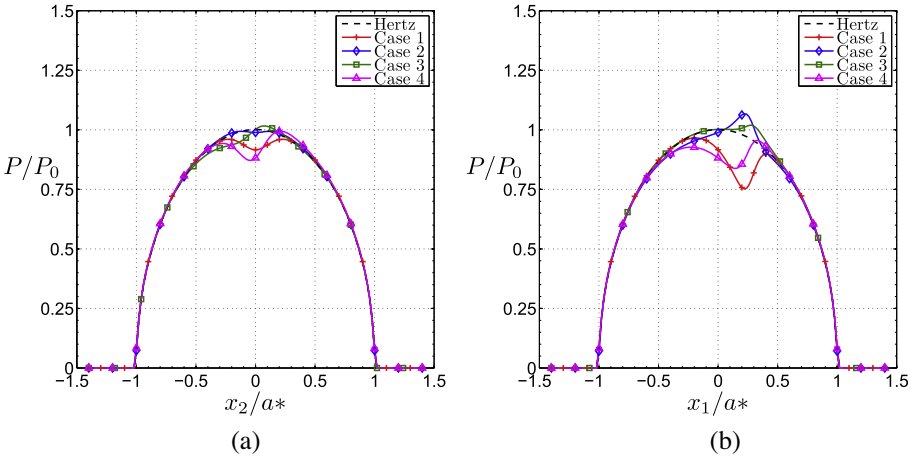

Fig. 18. Dimensionless contact pressure distribution for the heterogeneous solid in presence of an orthotropic tilted ellipsoidal inclusion ($a_1 = 0.4a^*,\ a_2 = a_3 = 0.1a^*,\ dx_3 = 0.4a^*,\ \theta = 45°$); (a) in the plane $x_1 = 0$ and (b) in the plane $x_2 = 0$.

Four material orientations are defined and studied this way:

- Case 1: $\varphi = 0°,\ \theta = 0°,\ \psi = 0°$, the orthotropy and contact axes coincide.
- Case 2: $\varphi = 90°,\ \theta = 45°,\ \psi = 90°$, the orthotropy and ellipsoid axes coincide.
- Case 3: $\varphi = 45°,\ \theta = 60°,\ \psi = 30°$.
- Case 4: $\varphi = -30°,\ \theta = 45°,\ \psi = 30°$.

The contact pressure distributions corresponding to the four cases are shown in Fig. 18(a) and (b).

One can see that depending on the orthotropic orientation relative to the contact orientation, the contact pressure value can either increase (Cases 1 and 4) or decrease (Cases 2 and 3). This is due to the fact that the inhomogeneity stiffness tensor associated to the contact axes varies widely in the four cases.

8. Conclusion

A numerical method has been proposed to model the effect of an heterogeneous ellipsoidal inclusion with arbitrary orientation on the solution of a three-dimensional contact problem. The elastic properties of the inhomogeneity can be either isotropic, orthotropic or fully anisotropic. The proposed method has been validated by performing a comparison with the results of a finite element model.

It is found that the presence of such an inclusion located below the contact surface modifies significantly to very significantly the

pressure distribution when its center is located at a depth up to 0.7 times the contact radius. An asymmetry of the pressure distribution is also observed when the axes of the ellipsoidal inclusion do not coincide with the contact problem axes. Still regarding the contact pressure distribution it was shown that both the dimensionless Young's modulus of the inclusion and the dimensionless bulk modulus have a very strong effect on the local contact pressure. In other terms the compressibility properties of the inclusion are as important as the dimensionless Young's modulus. A local peak of pressure up to 5 times the one in the absence of inclusion can be observed in some extreme configurations.

The normal and shear stresses at the interface between the inclusion and the matrix have also been investigated. In the configurations analyzed it was found that the normal stress is mostly compressive, whatever the elastic properties of the inclusion including when of ellipsoidal shape. Further work is now required to study more accurately what happens at the inclusion/matrix interface, as a function of the elastic properties of both materials, aiming at developing a decohesion model. Finally it should be pointed out that (i) the method can account for the interactions between close inclusions, and (ii) any geometry and material properties of the contacting bodies may be considered in the modeling (in other words the indenter does not have to be rigid and spherical).

Appendix A. Stress in a half-space due to a concentrated unit normal force at the surface origin (F_{ij})

$$F_{11}(x_1,x_2,x_3)=\frac{1}{2\pi}\left[\frac{1-2\nu}{r^2}\left(1-\frac{x_3}{\rho}\right)\frac{x_1^2-x_2^2}{r^2}+\frac{x_3x_2^2}{\rho^3}-\frac{3x_3x_1^2}{\rho^5}\right],$$

$$F_{22}(x_1,x_2,x_3)=F_{11}(x_2,x_1,x_3),$$

$$F_{33}(x_1,x_2,x_3)=-\frac{3}{2\pi}\frac{x_3^3}{\rho^5},$$

$$F_{12}(x_1,x_2,x_3)=\frac{1}{2\pi}\left[\frac{1-2\nu}{r^2}\left(1-\frac{x_3}{\rho}\right)\frac{x_1x_2}{r^2}+\frac{x_3x_2x_1}{\rho^3}-\frac{3x_3x_2x_1}{\rho^5}\right],$$

$$F_{13}(x_1,x_2,x_3)=-\frac{3}{2\pi}\frac{x_1x_3^2}{\rho^5},$$

$$F_{23}(x_1,x_2,x_3)=F_{12}(x_2,x_1,x_3),$$

where

$$r^2=x_1^2+x_2^2,\quad \rho=\sqrt{x_1^2+x_3^2+x_3^2}$$

with ν, the Poisson's ratio of the isotropic half-space.

Appendix B. Stresses in a half-space subject to normal pressure (M_{ij})

An isotropic half-space is submitted an uniform normal pressure σ^n in a discretized surface area of $2\Delta x_1\times 2\Delta x_2$ at the center point $P(x_1',x_2',0)$. The stress at an observation point $Q(x_1,x_2,x_3)$ is given by Zhou et al. (2009) and Johnson (1985):

$$\sigma_{ij}(x_1,x_2,x_3)=M_{ij}(x_1-x_1',x_2-x_2',x_3)\sigma^n(x_1,x_2),$$

$$\sigma_{ij}(x_1,x_2,x_3)=\frac{\sigma^n}{2\pi}[h_{ij}(\xi_1+\Delta x_1,\xi_2+\Delta x_2,\xi_3)-h_{ij}(\xi_1+\Delta x_1,\xi_2-\Delta x_2,\xi_3)+h_{ij}(\xi_1-\Delta x_1,\xi_2-\Delta x_2,\xi_3)-h_{ij}(\xi_1-\Delta x_1,\xi_2+\Delta x_2,\xi_3)],$$

where

$$\xi_i=x_i-x_i'.$$

The functions $h_{ij}()$ in Eq. (B1) are defined by

$$h_{11}(x_1,x_2,x_3)=2\nu\tan^{-1}\frac{x_2^2+x_3^2-\rho x_2}{x_1x_3}+2(1-\nu)\tan^{-1}\frac{\rho-x_2+x_3}{x_1}+\frac{x_1x_2x_3}{\rho(x_1^2+x_3^2)},$$

$$h_{22}(x_1,x_2,x_3)=h_{11}(x_2,x_1,x_3),$$

$$h_{33}(x_1,x_2,x_3)=\tan^{-1}\frac{x_2^2+x_3^2-\rho x_2}{x_1x_3}-\frac{x_1x_2x_3}{\rho}\left(\frac{1}{x_1^2+x_3^2}+\frac{1}{x_2^2+x_3^2}\right),$$

$$h_{12}(x_1,x_2,x_3)=-\frac{x_3}{\rho}-(1-2\nu)\log(\rho+x_3),$$

$$h_{13}(x_1,x_2,x_3)=-\frac{x_2x_3^2}{\rho(x_1^3+x_3^2)},$$

$$h_{23}(x_1,x_2,x_3)=h_{13}(x_2,x_1,x_3),$$

where

$$\rho=\sqrt{x_1^2+x_2^2+x_3^2}.$$

Appendix C. Normal displacement at the surface subject to normal pressure (K^n)

The contact between a sphere and an elastic half-space having respectively elastic constants (E_1,ν_1) and (E_2,ν_2), where the surface $x_3=0$ is discretized into rectangular surface area of $2\Delta_1\times 2\Delta_2$, is now considered. The initial contact point coincides with the origin of the Cartesian coordinate system (x_1,x_2,x_3). The relationship between the normal displacement at an observation point $P(\xi_1,\xi_2,0)$ and the pressure field at the center $Q(\xi_1',\xi_2',0)$ is built using the function K^n:

$$K^n(c_1,c_2)=\left[\frac{1-\nu_1^2}{\pi E_1}+\frac{1-\nu_2^2}{\pi E_2}\right]\sum_{p=1}^{4}K_p^n(c_1,c_2),$$

$$K_1^n(c_1,c_2)=(c_1+\Delta_1)\log\left(\frac{(c_2+\Delta_2)+\sqrt{(c_2+\Delta_2)^2+(c_1+\Delta_1)^2}}{(c_2-\Delta_2)+\sqrt{(c_2-\Delta_2)^2+(c_1+\Delta_1)^2}}\right),$$

$$K_2^n(c_1,c_2)=(c_2+\Delta_2)\log\left(\frac{(c_1+\Delta_1)+\sqrt{(c_2+\Delta_2)^2+(c_1+\Delta_1)^2}}{(c_1-\Delta_1)+\sqrt{(c_2+\Delta_2)^2+(c_1-\Delta_1)^2}}\right),$$

$$K_3^n(c_1,c_2)=(c_1-\Delta_1)\log\left(\frac{(c_2-\Delta_2)+\sqrt{(c_2-\Delta_2)^2+(c_1-\Delta_1)^2}}{(c_2+\Delta_2)+\sqrt{(c_2+\Delta_2)^2+(c_1-\Delta_1)^2}}\right),$$

$$K_4^n(c_1,c_2)=(c_2-\Delta_2)\log\left(\frac{(c_1-\Delta_1)+\sqrt{(c_2-\Delta_2)^2+(c_1-\Delta_1)^2}}{(c_1+\Delta_1)+\sqrt{(c_2-\Delta_2)^2+(c_1+\Delta_1)^2}}\right),$$

where

$$c_1=\xi_1-\xi_1'\quad\text{and}\quad c_2=\xi_2-\xi_2'.$$

Appendix D. Appendix D. Euler rotation matrix

$$R_Z(\varphi) = \begin{pmatrix} \cos\varphi & -\sin\varphi & 0 \\ \sin\varphi & \cos\varphi & 0 \\ 0 & 0 & 1 \end{pmatrix}.$$

$$R_Z(\psi) = \begin{pmatrix} \cos\psi & -\sin\psi & 0 \\ \sin\psi & \cos\psi & 0 \\ 0 & 0 & 1 \end{pmatrix}.$$

$$R_X(\alpha) = \begin{pmatrix} 1 & 0 & 0 \\ 0 & \cos\alpha & -\sin\alpha \\ 0 & \sin\alpha & \cos\alpha \end{pmatrix}.$$

$$P(\varphi, \alpha, \psi) = R_Z(\varphi) R_X(\alpha) R_Z(\psi).$$

References

Aderogba, K., 1976. On eigenstresses in a semi-infinite solid. Math. Proc. Cambridge Philos. Soc. 80 (3), 555–562.

Asaro, R., Barnett, D., 1975. The nonuniform transformation strain problem for an anisotropic ellipsoidal inclusion. J. Mech. Phys. Solids 23, 77–83.

Bagault, C., Nelias, D., Baietto, M.-C., 2012. Contact analyses for anisotropic half space: effect of the anisotropy on the pressure distribution and contact area. ASME J. Tribol. 134 (3), 031401 (8 p).

Bagault, C., Nelias, D., Baietto, M.C., Ovaert, T.C., 2013. Contact analyses for anisotropic half-space coated with an anisotropic layer: Effect of the anisotropy on the pressure distribution and contact area. Int. J. Solids Struct., 0020-7683 50 (5), 743–754.

Boucly, V., Nelias, D., Liu, S., Wang, Q., Keer, L., 2005. Contact analyses for bodies with frictional heating and plastic behaviour. ASME J. Tribol. 127 (2), 355–364.

Chaise, T., Nelias, D., 2011. Contact pressure and residual strain in 3D elasto-plastic rolling contact for a circular or elliptical point contact. J. Tribol. 133 (4), 041402-1.

Chaise, T., Nelias, D., Sadeghi, F., 2011. On the effect of isotropic hardening on the coefficient of restitution for single or repeated impacts using a semi-analytical method. Tribol. Trans. 54 (5), 714–722.

Chaise, T., Li, J., Nelias, D., Kubler, R., Taheri, S., Douchet, G., Robin, V., Gilles, P., 2012. Modelling of multiple impacts for the prediction of distortions and residual stresses induced by ultrasonic shot peening (USP). J. Mater. Process. Technol. 212, 2080–2090.

Chen, W., Wang, Q., Wang, F., Keer, L., Cao, J., 2008. Three-dimensional repeated elasto-plastic point contact, rolling and sliding. ASME J. Appl. Mech. 75, 021021-1–021021-12.

Chen, W., Liu, S., Wang, Q., 2008. FFT-based numerical methods for elasto-plastic contacts of nominally flat surfaces. ASME J. Appl. Mech. 75, 011022-1–011022-11.

Chiu, Y., 1977. On the stress field due to initial strains in a cuboid surrounded by an infinite elastic space. ASME J. Appl. Mech. 44, 587–590.

Chiu, Y., 1978. On the stress field and surface deformation in a half space with a cuboidal zone in which initial strains are uniform. ASME J. Appl. Mech. 45, 302–306.

Courbon, J., Lormand, G., Dudragne, G., Daguier, P., Vincent, A., 2005. Influence of inclusion pairs, clusters and stringers on the lower bound of the endurance limit of bearing steels. Tribol. Int. 36, 921–928.

Eshelby, J., 1957. The determination of the elastic field of an ellipsoidal inclusion and related problems. Proc. R. Soc. Lond. A241, 376–396.

Eshelby, J., 1959. The elastic field outside an elastic inclusion. Proc. R. Soc. Lond. A252, 561–569.

Eshelby, J., 1961. Elastic inclusions and inhomogeneities. Prog. Solid Mech. 2, 89–140.

Fulleringer, B., Nelias, D., 2010. On the tangential displacement of a surface point due to a cuboid of uniform plastic strain in a half-space. ASME J. Appl. Mech. 77 (2), 021014-1/7.

Gallego, L., Nelias, D., 2007. Modeling of fretting wear under gross slip and partial slip conditions. ASME J. Tribol. 129 (3), 528–535.

Gallego, L., Nelias, D., Jacq, C., 2006. A comprehensive method to predict wear and to define the optimum geometry of fretting surfaces. ASME J. Tribol. 128 (3), 476–485.

Gallego, L., Fulleringer, B., Deyber, S., Nelias, D., 2010a. Multiscale computation of fretting wear at the blade/disk interface. Tribol. Int. 43, 708–718.

Gallego, L., Nelias, D., Deyber, S., 2010b. A fast and efficient contact algorithm for fretting problems applied to fretting modes I, II and III. Wear 268, 208–222.

Gradshteyn, I. Ryzhik, Table of Integrals, Series and Products, Academic Press, 1965.

Jacq, C., Nelias, D., Lormand, G., Girodin, D., 2002. Development of a three-dimensional semi-analytical elastic–plastic contact code. ASME J. Tribol. 124 (4), 653–667.

Johnson, K.L., 1985. Contact Mechanics. Cambridge University Press.

Kabo, E., Ekberg, A., 2002. Fatigue initiation in railway wheels – a numerical study of the influence of defects. Wear 253, 26–34.

Kabo, E., Ekberg, A., 2005. Material defects in rolling contact fatigue of railway wheels-the influence of defect size. Wear 258, 1194–1200.

Kuo, C., 2007. Stress disturbances caused by the inhomogeneity in an elastic half-plane subjected to contact loading. Int. J. Solids Struct. 44, 860–873.

Kuo, C., 2008. Contact stress analysis of an elastic half-plane containing multiple inclusions. Int. J. Solids Struct. 45, 4562–4573.

Leroux, J., Nelias, D., 2011. Stick-slip analysis of a circular point contact between a rigid sphere and a flat unidirectional composite with cylindrical fibers. Int. J. Solids Struct. 48, 3510–3520.

Leroux, J., Fulleringer, B., Nelias, D., 2010. Contact analysis in presence of spherical inhomogeneities within a half-space. Int. J. Solids Struct. 47, 3034–3049.

Liu, S., Wang, Q., 2005. Elastic fields due to eigenstrains in a half-space. ASME J. Tribol. 72, 871–878.

Liu, S., Wang, Q., Liu, G., 2000. A versatile method of discrete convolution and FFT (DC-FFT) for contact analyses. Wear 243 (1–2), 101–111.

Love, A.E.H., 1952. A Treatise on the Mathematical Theory of Elasticity, fourth ed. Cambridge University Press.

Mindlin, R., Cheng, D., 1950. Thermoelastic stress in the semi-infinite solid. J. Appl. Phys. 21, 931–933.

Moschovidis, Z., Mura, T., 1975. Two-ellipsoidal inhomogeneities by the equivalent inclusion method. ASME J. Appl. Mech. 42, 847–852.

Mura, T., 1987. Micromechanics of Defects in Solids, second ed. Kluwer Academic Publishers.

Mura, T., Furuhashi, R., 1984. The elastic inclusions with a sliding interface. ASME J. Appl. Mech. 51, 308–310.

Nelias, D., Dumont, M.-L., Champiot, F., Vincent, A., Girodin, D., Fougres, R., Flamand, L., 1999. Role of inclusions, surface roughness and operating conditions on rolling contact fatigue. ASME J. Tribol. 121 (2), 240–251.

Nelias, D., Antaluca, E., Boucly, V., Cretu, S., 2007. A 3D semi-analytical model for elastic-plastic sliding contacts. ASME J. Tribol. 129 (4), 761–771.

Nelias, D., Antaluca, E., Boucly, V., 2007. Rolling of an elastic ellipsoid upon an elastic–plastic flat. J. Tribol. 129 (4), 791–800.

Nugent, E., Calhoun, R., Mortensen, A., 2000. Experimental investigation of stress and strain fields in a ductile matrix surrounding an elastic inclusion. Acta Mater. 48, 1451–1467.

Rodriguez-Tembleque, L., Buroni, F., Abascal, R., Saez, A., 2013. Analysis of FRP composites under frictional contact conditions. Int. J. Solids Struct., 0020-7683 50, 3947–3959.

Seo, T., Mura, T., 1970. The elastic field in half space due to ellipsoidal inclusions with uniform dilatational eigenstrains. ASME J. Appl. Mech. 46, 568–572.

Vignal, V., Oltra, R., Josse, C., 2003. Local analysis of the mechanical behavior of inclusions-containing stainless steels under strstrain conditions. Scr. Mater. 49, 779–784.

Voskamp, A., 1985. Material response to rolling contact loading. ASME J. Tribol. 107, 359–366.

Walpole, L., 1967. The elastic field of an inclusion in an anisotropic medium. Proc. R. Soc. Lond. A300, 270–288.

Wang, F., Keer, L., 2005. Numerical simulation for three dimensional elastic–plastic contact with hardening behavior. ASME J. Tribol., 0742-4787 127 (3), 494–502.

Wang, F., Block, J., Chen, W., Martini, A., Keer, L., Wang, Q., 2009. A multi-scale model for the simulation and analysis of elasto-plastic contact of real machined surfaces. ASME J. Tribol. 131, 021409-1–021409-6.

Willis, J., 1964. Anisotropic elastic inclusion problems. Q. J. Mech. Appl. Math. 17 (2), 157–174.

Zhou, K., Chen, W., Keer, L., Wang, Q., 2009. A fast method for solving three-dimensional arbitrarily shaped inclusions in a half space. Comput. Methods Appl. Mech. Eng. 198 (9–12), 885–892.

Zhou, K., Chen, W., Keer, L., Ai, X., Sawamiphakdi, K., Glaws, P., Wang, Q., 2011a. Multiple 3D inhomogeneous inclusions in a half space under contact loading. Mech. Mater. 43, 444–457.

Zhou, K., Keer, L., Wang, Q., 2011b. Semi-analytic solution for multiple interacting three-dimensional inhomogeneous inclusions of arbitrary shape in an infinite space. Int. J. Numer. Methods Eng. 87, 617–638.

Zhou, K., Keer, L., Wang, Q., Ai, X., Sawamiphakdi, K., Glaws, P., Paire, M., Che, F., 2012. Interaction of multiple inhomogeneous inclusions beneath a surface. Comput. Methods Appl. Mech. Eng. 217–220, 25–33.

Zhou, K., Hoh, H.J., Wang, X., Keer, L.M., Pang, J.H.L., Song, B., Wang, Q.J., 2013. A review of recent works on inclusions. Mech. Mater., 0167-6636 60, 144–158.